scientific reports

Check for updates

OPEN

Genuine anodic and cathodic current components in cyclic voltammetry

Valentin Mirceski[1,2,3]✉, Dariusz Guziejewski[1] & Rubin Gulaboski[4]

Implicit anodic and cathodic current components associated with the real net current at a given potential of a simple quasireversible electrode reaction can be accurately estimated using basic mathematical modeling within the framework of Butler-Volmer electrode kinetics. This methodology requires only prior knowledge of the formal potential of the dissolved redox couple, offering direct insight into the electrode kinetics. The proposed approach facilitates a unique transformation of a conventional cyclic voltammogram, allowing the replacement of the common, net current with authentic anodic and cathodic current components. This simple methodology introduces a novel perspective in analyzing voltammetric data, particularly enabling the kinetic characterization of fast, seemingly electrochemically reversible electrode processes on macroscopic electrodes at slow scan rates. Theoretical predictions are experimentally demonstrated using the electrode reaction for the reduction of the hexaammineruthenium(III) complex, serving as an example of one of the fastest electrode processes involving a dissolved redox species.

Keywords Cyclic voltammetry, Electrode kinetics, Implicit anodic and cathodic current components

Cyclic voltammetry is undeniably the most fundamental and widely utilized technique in electrochemistry[1]. Its effectiveness lies in its simplicity of implementation and its ability to provide insights into intrinsic aspects of the physicochemical system under study, including the chemical mechanism, thermodynamics and kinetics of the interfacial electron transfer (i.e., the electrode reaction), as well as the physicochemical processes coupled to or arising from it (i.e., chemical reactions, adsorption phenomena etc.). The triangular potential excursion around the formal potential $E^{0'}$of the studied redox couple Ox/Red is designed to distinguish the features of the oxidative (Red to Ox) and reductive (Ox to Red) reactions separately. Although the oxidation and reduction electrode reactions of a single redox couple represent distinct electrochemical events, they constitute a unified reaction system (i.e., the electrode reaction represented by the scheme Red $\leftrightarrows$ Ox + e), akin to a chemically reversible system A $\leftrightarrows$ B, consisting of two different chemical reactions (A $\dashrightarrow$ B and B $\dashrightarrow$ A) occurring simultaneously.

In the case of a truly reversible electrode system, the triangular variation of the potential during the cyclic voltammetric experiment can be interpreted as the shifting of the redox equilibrium between Ox/Red species at the electrode surface dictated by the electrode potential. This equilibrium drift is achieved by precisely varying the activity of electrons of the working electrode (i.e., the electrode potential) involved in the interfacial electron transfer. If the electrode reaction is influenced by the kinetics of the interfacial electron exchange, the triangular potential variation aims to independently accelerate each of the two distinct processes (oxidation and reduction). In other words, when conducting the experiment with only one form of the redox couple initially present (e.g., Red species), the first half of the experiment focuses on accelerating the oxidation reaction (i.e., Red $\dashrightarrow$ Ox + e), while the opposite is true for the second half of the cyclic voltammetric experiment. This is feasible due to the empirical observation that anodic and cathodic rate constants depend on the electrode potential, considered in either theoretical framework used for rationalizing the experiment (i.e., Butler-Volmer[2–6] or Markus-Hush kinetic model[7–11]).

Despite the attempt to resolve the two distinct processes as much as possible, the experimental reality is that both oxidation and reduction processes proceed simultaneously. The only experimentally accessible parameter

[1]Department of Instrumental Analysis, University of Lodz, Pomorska 163, 90-236 Łódź, Poland. [2]Institute of Chemistry, Faculty of Natural Sciences and Mathematics, Ss Cyril and Methodius University in Skopje, P.O. Box 162, 1000 Skopje, Republic of North Macedonia. [3]Research Center for Environment and Materials, Macedonian Academy of Sciences and Arts, Bul. Krste Misirkov 2, 1000 Skopje, Republic of North Macedonia. [4]Faculty of Medical Sciences, Goce Delcev University, Stip, Republic of North Macedonia. ✉email: valentin.mircheski@chemia.uni.lodz.pl

is the net current, which represents the difference between the implicit anodic and cathodic current components thus representing an overall effect of two distinct processes. The situation is particularly complicated close to the formal potential as both anodic and cathodic reactions proceed at a significant rate. Yet, crucial parameters of a cyclic voltammogram (peak currents and peak potentials) are actually measured close to the formal potential of the studied redox couple.

Thus, on the basis of our recently proposed methodology[12], the primary focus of this study is to address whether a conventional cyclic voltammetric experiment can be processed in a certain way to unveil separate, implicit current components while measuring the only experimentally accessible net current. Furthermore, if the electrode reaction of a dissolved redox couple is very fast and the net peak currents cease to depend on the electrode kinetics (i.e., apparently reversible electrode reaction), does it mean that the implicit current components are also insensitive to the electrode kinetics? The following simple analysis in the present study addresses these basic questions which seems to be not trivial, demonstrating that distinct, implicit current components can be unambiguously revealed, by taking advantage of the convolution integration of the current[13–16].

Experimental

All chemicals utilized were of analytical grade purity, sourced from Merck. All solutions were meticulously prepared using deionized water obtained via the Polwater DL-3 purification system. Stock solution of 1 mM $[Ru(NH_3)_6]Cl_3$ was prepared by dissolving in aqueous solution of 1 mol/L KNO_3 as the latter served as a supporting electrolyte and it was used as prepared after oxygen removal.

An Autolab potentiostat model PGSTAT302N controlled by the Nova software (v. 2.1.5, both Metrohm Autolab B.V.) was used to conduct all experiments under conditions of square-wave and linear sweep cyclic voltammetry, using glassy carbon electrode (BASi Inc.) with a surface area 7.1×10^{-6} m^2 as a working electrode, Ag/AgCl (3 mol/L KCl) as a reference, and a platinum wire as a counter electrode. All experiments were conducted at room temperature of 20 °C.

The linear sweep voltammetry was conducted by using the module SCAN250, with a potential resolution of the current recording of 2.44 mV. The cyclic voltammograms have been smoothed by Savitzky Golay mode with polynomial order 2 and smooth level 2 (i.e., the bin size is 5), while the baseline correction have been done with a linear mode.

Results and discussion

Derivation of the implicit current components

Let us consider a simple one-electron reaction at a stationary, planar, macroscopic electrode of a dissolved redox couple, free of any adsorption phenomena and coupled chemical reactions:

$$\mathrm{Red(sol)} \rightleftarrows \mathrm{Ox(sol)} + \mathrm{e} \tag{1}$$

The solutions for the surface concentrations of redox species are well known[17]:

$$c_{\mathrm{Red}}(0,t) = c^{*} - I_{con}(t) \tag{2}$$

and

$$c_{\mathrm{Ox}}(0,t) = I_{con}(t) \tag{3}$$

here $I_{con}(t) = \int_0^t \frac{I(\tau)}{FA\sqrt{D}} \frac{d\tau}{\sqrt{\pi(t-\tau)}}$ is the convolution, or semi-integral, c^{*} is the bulk concentration of Red species initially present in the solution, D is the common diffusion coefficient, and other symbols have their common meaning. Equations (2) and (3) follow from the solution of the diffusion equation only, thus reflecting solely the process of diffusion. In another words, convolution integral $I_{con}(t)$ is mathematical representation the diffusion effect in the course of the voltammetric experiment. It is however important to recall that the diffusion is driven by the concentration gradients prompted by the electrode reaction.

If the electrode reaction is kinetically controlled, then the Butler-Volmer equation holds at the electrode surface, relating the current with the surface concentrations $c_i(0,t)$, electrode potential, and kinetic parameters:

$$\frac{I(t)}{FA} = k_s \exp(\beta\phi)\left[c_{\mathrm{Red}}(0,t) - c_{\mathrm{Ox}}(0,t)\exp(-\phi(t))\right] \tag{4}$$

Specifically, k_s is the standard rate constant (cm s^{-1}), β is the anodic electron transfer coefficient, and $\phi(t) = \frac{F}{RT}\left(E(t) - E^{\circ'}\right)$ is dimensionless potential defined versus the formal potential ($E^{\circ'}$) of the electrode reaction. Combining kinetic Eq. (4), which explains the phenomena at the electrode surface, with Eq. (2) and (3), which describe the mass transfer phenomena prompted by the electrode reaction, provide the theoretical basis for understanding electrochemical experiments under chronoamperometric and voltammetric conditions.

Equation (4) is derived assuming, that implicit anodic $I_a(t)$ and cathodic $I_c(t)$ current components determine the net $I(t)$, experimentally measurable, current:

$$I(t) = I_a(t) + I_c(t) \tag{5}$$

where

$$I_a(t) = FAk_s \exp(\beta\phi(t))[c_{\mathrm{Red}}(0,t))] \tag{6}$$

$$I_c(t) = -FAk_s\exp[-(1-\beta)\phi(t)]c_{\mathrm{Ox}}(0,t) \tag{7}$$

Note the negative sign in front of the cathodic current in Eq. (7), thus the net current $I(t)$ in Eq. (5) is represented as a sum of the anodic and cathodic current components. Clearly, substituting Eq. (2) into (6), and (3) into (7), the anodic and cathodic current components can be related with the total, net current through the convolution integral $I_{con}(t)$ as follows:

$$I_a(t) = FAk_s\exp(\beta\phi(t))\left(c^* - I_{con}(t)\right) \tag{8}$$

$$I_c(t) = -FAk_s\exp[-(1-\beta)\phi(t)]I_{con}(t) \tag{9}$$

For the sake of clarity let us emphasise that though convolutive integral is required to calculate implicit current components $I_a(t)$ and $I_c(t)$, they are just common, not convolutive currents, making clear difference of the present method with the convolutive voltammetry, where the convolutive current $I_{con}(t)$ is analysed as a function of the potential[13–16].

Considering the last two Eqs. (8) and (9), it follows that the ratio of $I_a(t)/I_c(t)$ results in a relation in which kinetic parameters (k_s and β) cancel out:

$$\frac{I_a(t)}{I_{c(t)}} = -\frac{c^* - I_{con}(t)}{\exp(-\phi(t))I_{con}(t)} \tag{10}$$

Equation (10) is the central equation of the current study, revealing that the ratio of current components is clearly contingent upon the potential alone. Solving the system of Eqs. (5) and (10) straightforwardly yields the anodic and cathodic current components at any moment during the voltammetric experiment. This necessitates the initial calculation of the convolution integral and prior knowledge of the formal potential of the redox couple, without any prior knowledge of the electrode kinetic parameters (k_s and β). Once being revealed, the implicit current components lead straightforwardly to the intrinsic kinetic parameters, as clearly shown by Eqs. (8) and (9). Such a theoretical consideration is generally valid for any voltammetric and chronoamperometic experiment.

Let us now consider theoretically a simple experiment under conditions of linear sweep cyclic voltammetry. The response can be calculated in a dimensionless current domain, according to the numerical step-function method[18]:

$$\Psi_m = \frac{\kappa\exp(\beta\phi_m)\left[1 - \frac{2\sqrt{dEF}}{\sqrt{\pi RT}}\left(1+\exp(-\phi_m)\right)\sum_{j=1}^{m-1}\Psi_j S_{m-j+1}\right]}{1 + \frac{2\kappa\sqrt{dEF}}{\sqrt{\pi RT}}\left(1+\exp(-\phi_m)\right)} \tag{11}$$

where the dimensionless current is defined as $\psi(t) = \frac{I(t)\sqrt{RT}}{FAc^*\sqrt{DvF}}$, $\kappa = k_s\sqrt{\frac{RT}{DvF}}$ is the dimensionless electrode kinetic parameter, dE is the potential increment, and $S_m = \sqrt{m} - \sqrt{m-1}$ is the numerical integration parameter with a serial number m. Once the net current ψ is known (either being calculated with the aid of Eq. (11), or in the real experiment, measuring the current at each time t of the experiment), the system of Eqs. (5) and (10) can be used to obtain the cathodic and anodic implicit current components in a dimensionless form:

$$\Psi_{c,m} = \frac{\Psi_m b_m}{b_m - a_m} \tag{12}$$

$$\Psi_{a,m} = \Psi_m - \Psi_{c,m} \tag{13}$$

where $a_m = 1 - \frac{2\sqrt{dEF}}{\sqrt{RT\pi}}\Psi con_m$, $b_m = \frac{2\sqrt{dEF}\exp(-\varphi_m)}{\sqrt{RT\pi}}\Psi con_m$, and $\Psi con_m = \sum_{j=1}^{m}\Psi_j S_{m-j+1}$ is the numerical form of the convolution integral.

The initial outcome of such calculations is illustrated in Fig. 1, where the blue curves represent typical dimensionless conventional cyclic voltammograms for different degree of electrochemical reversibility, encompassing sluggish (electrochemically irreversible), quasireversible, and fast, apparently electrochemically reversible electrode reaction, calculated by means of Eq. (11). Once the net currents are known, and using only the formal potential values, one can calculate the implicit anodic and cathodic current components in the course of the voltammetric experiment by means of Eqs. (12) and (13). For each half-cycles of the voltammetric experiment corresponding implicit anodic and cathodic current components are calculated. Figure 1 illustrates a revised version of cyclic voltammograms, showcasing the sole anodic (red curves) and cathodic (green curves) current components associated with the forward (anodic) and reverse (cathodic) half-cycles of the virtual voltammetric experiment.

In instances where the electrode reaction is sluggish, characterized by the electrode kinetic parameter $\kappa = 0.1$ ($\log(\kappa) \leq -1$), the sole current components align seamlessly with the net current, as evidenced in Fig. 1A. This alignment could serve as a real criterion for a precise defining of the electrochemical irreversibility in terms of the electrode kinetics. Under these conditions, the implicit anodic component ψ_a is identical with the net current in the course of the forward, anodic potential scan, implying that the contribution of the implicit cathodic current component in the course of the forward scan is insignificant. An analogous discussion can be given for the reverse, cathodic potential scan.

The relationship between the current components and the net current undergoes significant changes for typically quasireversible and fast (apparently electrochemically reversible) electrode reactions, as depicted in

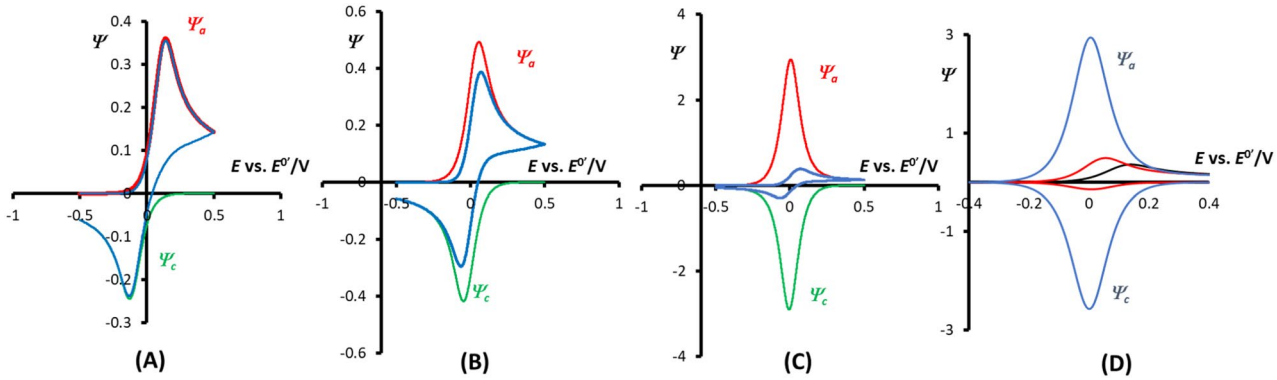

Figure 1. Typical dimensionless cyclic voltammograms for different degree of electrochemical reversibility (blue curves), including the sole anodic (Ψ_a; red curves) and cathodic (Ψ_c; green curves) implicit current components corresponding to the anodic and cathodic half-potential circles, respectively. The electrode kinetic parameter κ is 0.1 (**A**); 0.5 (**B**), and 5.5 (**C**). Panel (**D**) shows current components corresponding to the forward scan of the cyclic voltammetric experiment only, for electrode kinetic parameter values corresponding to panels (**A**)–(**C**). The electron transfer coefficient is $\beta = 0.5$, potential increment is $dE = 0.1$ mV, and temperature is $T = 298.15$ K.

Fig. 1B,C, respectively. Specifically, for a quasireversible scenario ($-1 \le \log(\kappa) \le 1$), the current components already surpass the net current, as illustrated in Fig. 1B ($\kappa = 0.5$; $\log(\kappa) = -0.3$). During the forward, anodic potential scan, the implicit anodic current component (Ψ_a) is larger than the net current. This implies that the implicit cathodic current component is also significant, resulting in a lower overall net current due to their difference. It is important to note that the cathodic current component (Ψ_c) corresponding to the forward potential scan is not shown on the plot for the sake of presentation simplicity. Similarly, for analogous reasons, the implicit cathodic current component corresponding to the reverse potential scan of the experiment is larger than the net cathodic current (green curve in Fig. 1B).

The discrepancy between the net and current components becomes significant when the electrode reaction is very fast ($\log(\kappa) > 0.5$), as depicted in Fig. 1C. For $\kappa = 5.5$, the peak current of the implicit anodic current component (Ψ_a) is almost an order of magnitude larger than the net anodic peak current of the conventional cyclic voltammogram (compare red and blue curves in Fig. 1C). This indicates that the electrode reaction Red ⇢ Ox + e proceeds rapidly, generating a highly intensive anodic current component. However, simultaneously, the reverse reaction Ox + e ⇢ Red occurs at a comparable rate, resulting in an intensive implicit cathodic current component (not shown). Thus, the overall effect is represented by a relatively low net current in the course of the forward potential scan. A similar discussion is relevant to the reverse, cathodic potential scan of the experiment.

For the sake of simplification, the analysis of the implicit anodic and cathodic current components could be restricted only to the initial, forward scan of the cyclic voltammetric experiment, as shown in Fig. 1D. Such analysis reveals the degree of electrochemical reversibility in both qualitative and quantitative terms.

Analysis of the implicit current components in the apparently reversible kinetic region

To unlock the genuine potential of the proposed methodology, one must scrutinize electrode reactions that are very fast and apparently electrochemically reversible. The conventional cyclic voltammograms depicted in Fig. 2A illustrate this progression, ranging from a very fast quasireversible electrode process ($\kappa = 2.53$) to apparently reversible electrode processes ($\kappa > 5$). Within this kinetic range, the conventional cyclic voltammograms appear to be identical, seem to become independent of the electrode kinetics and predominantly affected by the mass transfer only.

For an in-depth analysis of the behavior of implicit current components in the apparently reversible kinetic region, we propose an approach which resembles the reasoning of differential voltammetric techniques[19,20]. For this purpose, we use the implicit current components associated with the forward, anodic potential scan of the cyclic voltammetry only, and by analogy with differential voltammetric techniques, we define a differential current as $I_{dif}(t) = I_a(t) - I_c(t)$. Recalling the definitions of the current components through Eqs. (8) and (9), the expression for the differential current is given by:

$$I_{dif}(t) = FAk_s e^{\beta\phi(t)}\left[c^* - I_{con}(t)\left(1 - e^{-\phi(t)}\right)\right] \tag{14}$$

The reason for introducing the differential current is that it has unique features, which are not attributed to the conventional, net current. Specifically, at the formal potential ($E = E^{\circ'}$; $\phi = 0$), the differential current equals $I_{dif} = FAc^*k_s$. Obviously, under these conditions the convolution integral is cancelled out in Eq. (14), removing the effect of the mass transport in this artificial current component. In addition, the differential current is becoming independent on the electron transfer coefficient. It follows that $I_{dif}\left(E = E^{\circ'}\right)$ represents the exchange current for equilibrium conditions of the studied redox couple. Expressing this in a dimensionless form is $\Psi_{dif}\left(E = E^{\circ'}\right) = \kappa$.

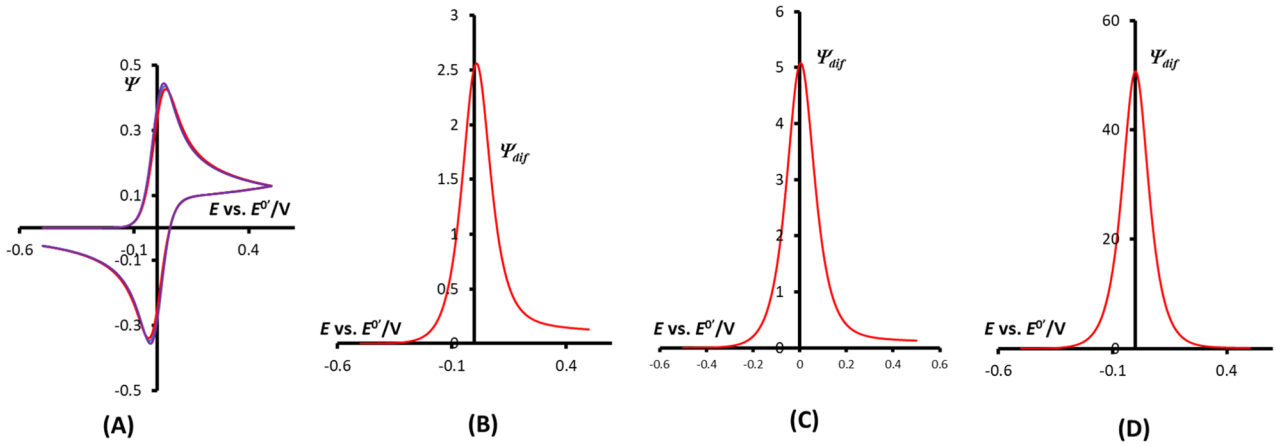

Figure 2. (**A**) Conventional cyclic voltammograms of very fast quasireversible electrode reaction characterized with the electrode kinetic parameter κ of 2.53; 5.1, and 50.1 (curves are overlapped). Panels (**B**–**D**) showcase differential current component (Ψ_{dif}) associated with the anodic half-cycle of the cyclic voltammogram simulated for an increasing degree of the electrochemical reversibility. The electrode kinetic parameter κ is 2.53 (**B**), 5.1 (**C**), and 50.1 (**D**). The other conditions are the same as for Fig. 1.

For better clarity of these profound features of the differential current, which could be calculated only by previous knowledge of the implicit anodic and cathodic current components, let us write an equation for the common, net current, analogous to Eq. (14):

$$I(t) = FAk_s e^{\beta\phi(t)}\left[c^* - I_{con}(t)\left(1 + \mathrm{e}^{-\phi(t)}\right)\right] \tag{15}$$

The difference between Eqs. (14) and (15) lies solely in the sign within the small bracket. It is easy to see that at $E = E^{\circ'}$ ($\phi = 0$) the convolution integral (i.e., the effect of diffusion) cannot be cancelled out in the common net current $I(t)$ (Eq. (15)). Thus, it remains affected by both diffusion and electrode kinetics, and their intricate complex interplay is the sole origin of complexity in the interpretation of the voltammetric data in general.

The analysis of an electrode reaction by means of differential current is illustrated in Fig. 2B–D, depicting the evolution of the differential current during the forward scan of the cyclic voltammetry. Notably, when the electrode reaction is rapid and apparently reversible, the differential current component calculated aligns at the formal potential (Fig. 2C,D). Its peak current provides a direct indication of the electrode kinetic parameter κ (note the difference in the scale of the ordinate in Fig. 2B–D). Therefore, the data shown in Fig. 2 clearly suggest that the proposed methodology enables the estimation of rapid electrode kinetics using standard macroscopic electrodes, which seems to be a unique virtue of the present methodology. On the other hand, the peak potential of the differential current depends on the electron transfer coefficient, enabling straightforward estimation of this parameter. For instance, for a very fast reaction associated with $\kappa = 50$, the dependence of the peak potential of the differential current and the anodic electron transfer coefficient β is linear, associated with the following linear regression line: $E_p = 0.115\ \beta$ -0.056 ($R^2 = 0.999$), over the range of β values from 0.2 to 0.8. Therefore, the analysis of the differential current component provides a means for simple, fast, and unambiguous estimation of both standard rate constant and the electron transfer coefficient.

Limitations of the method

The distinctive feature of the proposed method for elucidating the kinetic parameters of exceedingly rapid, ostensibly reversible electrode reactions must be scrutinized critically in relation to a genuinely reversible electrode reaction. Let us revisit the remarkably fast electrode reaction associated with the electrode kinetic parameter $\kappa = 50$. This high value of the electrode kinetic parameter corresponds to an electrode reaction with, for instance, a standard rate constant of $k_s = 0.1$ cm s^{-1}, diffusion coefficient of $D = 5 \times 10^{-6}$ cm^2 s^{-1} under experiment scan rate of $\nu = 20$ mV s^{-1}. Consequently, the electrode reaction falls comfortably within the apparent reversible kinetic region, where the peak currents of the conventional cyclic voltammogram are virtually independent of the electrode kinetics. In addition, let us now presume that the electron transfer behaves as a truly thermodynamically reversible process, described by the Nernst equation. The cyclic voltammograms corresponding to these two cases are compared in Fig. 3A and appear to be identical over the entire potential window. Applying Eqs. (12) and (13) to the voltammogram associated with $\kappa = 50$ yields well-defined anodic and cathodic current components, while the peak current of the differential current component is equal to κ, as discussed previously (cf. Fig. 2D). However, attempting to apply the same formulas (12) and (13) to the voltammogram of a truly reversible electrode reaction obeying the Nernst equation at any potential of the voltammetric experiment (e.g., ferrocene/ferrocenium redox couple) does not yield any reasonable data. Consequently, the net current of a truly reversible electrode reaction cannot be broken down into separate anodic and cathodic current components.

In a meticulous consideration of these theoretical data, a critical question arises: How identical are the net current data of a truly reversible electrode reaction and an apparently reversible electrode reaction, as implied

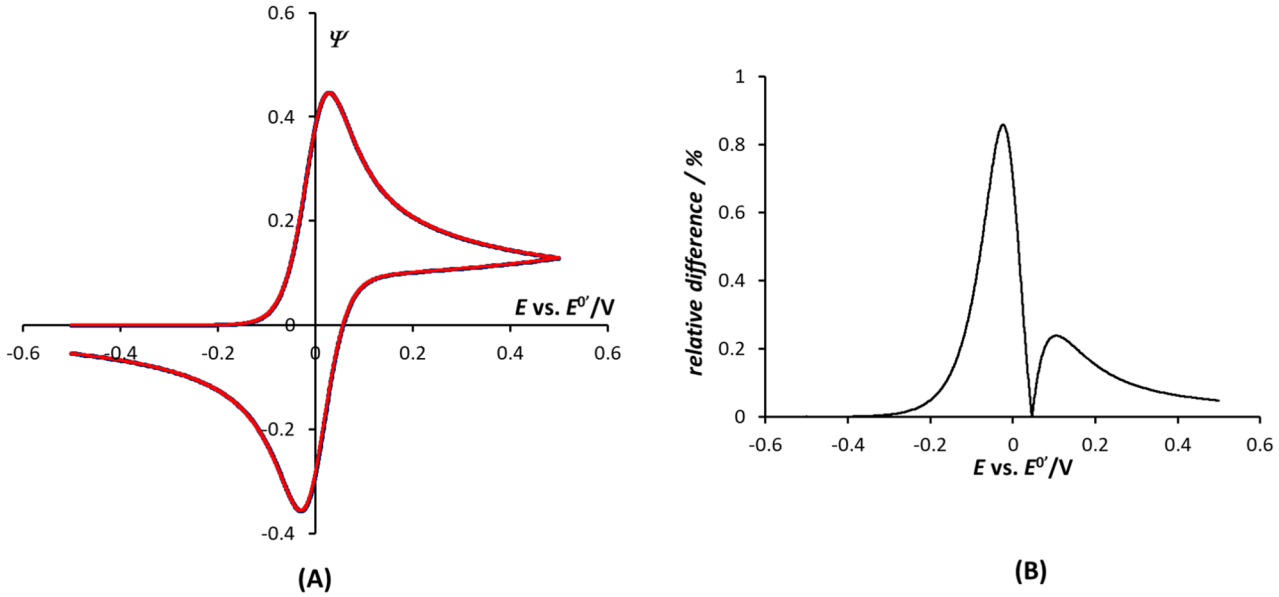

Figure 3. (**A**) Conventional cyclic voltammograms of very fast, apparently reversible electrode reaction characterized with the electrode kinetic parameter $\kappa = 50.1$ (red circles) and true reversible electrode reaction (blue solid line). (**B**) Relative variance between the currents of the voltammograms from panel (**A**) calculated for the first anodic half-cycle, calculated as $\frac{|\Psi(\kappa=50)-\Psi(rev)|}{|\Psi(\kappa=50)|}100\%$.

by Fig. 3A? The relative variance in the currents of these two voltammograms for the first half of the cyclic voltammetry is plotted in Fig. 3B. It is evident that they slightly differ (up to 1%) at the very beginning of the rising part of the voltammogram. Specifically, at low potentials, when the driving force of the electrode reaction is low enough, the electrode kinetics of the quasireversible electrode reaction still plays a role (red circles in Fig. 3A), being a slower step relative to diffusional mass transfer. Such an effect is completely absent in a truly reversible electrode reaction (black line in Fig. 3A). Therefore, these small differences between the very fast, apparently reversible, and the truly reversible reaction are of critical importance.

Considering that even tiny differences in the net currents play a decisive role in the successful application of the method, it is reasonable to anticipate that the noise from the current, an inevitable artefact in a real experiment, will hold significant importance. In order to investigate this effect through simulations, uniformly distributed noise was introduced to the recurrent formula (11) for calculating the net current, and the results are presented in Fig. 4. The noisy current was simulated by the extending the recurrent formula (11) as follows:

$$\Psi(noise)_m = \frac{\kappa \exp(\beta\phi_m)\left[1 - \frac{2\sqrt{dEF}}{\sqrt{\pi RT}}\left(1+\exp(-\phi_m)\right)\sum_{j=1}^{m-1}\Psi(noise)_j S_{m-j+1}\right]}{1+\frac{2\kappa\sqrt{dEF}}{\sqrt{\pi RT}}\left(1+\exp(-\phi_m)\right)} + Noise_m \qquad (22)$$

where $Noise_m$ is a function generating random numbers with a uniform distribution within the interval defined by the noise percentage, relative to the current measured at the lower foot of the idealized voltammograms (i.e., percentage of the current calculated by the recurrent formula (11) at potentials at least 200 mV less than the formal potential). The added noise at the beginning of the voltammogram propagates throughout the simulation due to the recurrent nature of Eq. (22). The analysis presented in Fig. 4 corresponds to an experimental scenario examining a very fast electrode reaction ($\kappa = 50$) under varying noise levels ranging from 1 to 5%. Panels A–C illustrate the anodic and cathodic current components derived from the raw, noisy data, referring to the forward scan of the cyclic voltammetric experiment. Evidently, processing the raw data accentuates the noise in both the anodic and cathodic current components, as a consequence of the convolution (summation) procedure. However, the overall morphology, peak currents, and peak potentials of both implicit current components remain virtually unaffected. To substantiate this claim, Fig. 4D presents the implicit current components estimated from the idealized, noise-free net currents. The peak currents and potentials, crucial for estimating the kinetic parameters, are virtually identical between the noisy and idealized data, demonstrating the robustness of the method.

Yet, the noise effect should be mitigated by smoothing the net currents before applying Eqs. (12) and (13), as well as by filtering and smoothing the obtained data for both anodic and cathodic implicit current components, while a plethora of tools are available for such a purpose[21,22]. An example of such procedure is given in Fig. 4E, including the initial smoothing of the raw data with the noise of 1%, and filtering and smoothing of the obtained anodic and cathodic implicit current components by means of the function "*medsmooth*" of the Mathcad software[23]. Let us note that the "medsmooth" function performs median filtering. It is the most robust among smoothing functions because it is less susceptible to influence from outliers. However, it tends to smooth out sharp features in the data. One can contrast this approach with Gaussian kernel smoothing or localized least-squares smoothing methods. In addition, Fig. 4E compares the processed data (dotted lines) with the idealized, noise free data, illustrating the effectiveness of the smoothing procedure. Importantly, Fig. 4E also displays the

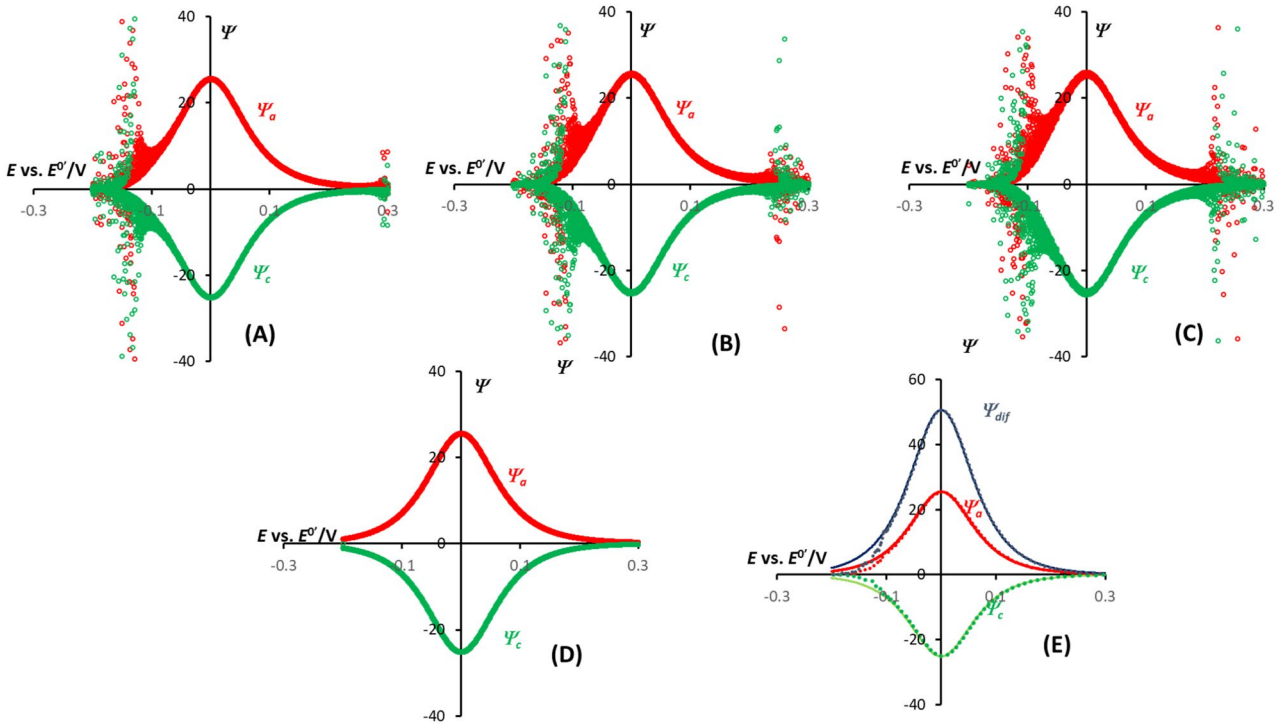

Figure 4. Anodic (Ψ_a, red curves) and cathodic (Ψ_c, green curves) implicit current components calculated from a noisy net current of a very fast, apparently reversible electrode reaction with the electrode kinetic parameter of $\kappa = 50$. For the sake of simplicity only the first half-cycle of the conventional cyclic voltammograms was considered. The level of noise, with a uniform distribution, was 1% (**A**), 3% (**B**) and 5% (**C**) relative to the net current measured at the lower foot of the cyclic voltammogram. Panel (**D**) displays the anodic and cathodic current components calculated from idealized, noise-free net currents. Panels (**E**) compares implicit current components estimated from net current with 1% noise, after smoothing the row data and smoothing the implicit current components (doted lines), with data calculated from idealized, noise-free net currents (full lines). The blue lines correspond to differential (ψ_{dif}) component. The smoothing of the noise net current was performed by applying "*medsmooth*" function of Mathcad[23], with a weight of 5 in averaging the raw data.

differential current component, suggesting that in the presence of noise, the proposed method leads to reliable estimation of the standard rate constant (from the peak current of the differential component) and the electron transfer coefficient (from the peak potential of the differential component).

Experimental verification

The characterization of electrode kinetics, besides employing scanning electrochemical microscopy[24], commonly utilizes cyclic voltammetry and electrochemical impedance spectroscopy[25]. Various methodologies are employed when applying linear sweep potential in studies, as detailed by Nicholson[26], Klingler-Kochi[27], or Gileadi[28]. Additionally, the development of (ultra)microelectrodes was prompted for the purpose of evaluating heterogeneous electron transfer kinetics of very fast processes by changing the regime of diffusion to be faster relative to the electron transfer[29].

Electrode reaction of hexaammineruthenium(III) complex is one of the fastest electrode reactions of a dissolved redox couple[24], being a perfect example of apparently electrochemically reversible process under common (slow scan rates) voltammetric conditions. Typical cyclic voltammogram for the reduction of ruthenium system is shown in Fig. 5A, exhibiting all characteristics of an electrochemically reversible electrode reaction of a dissolved redox couple. Over the scan rate interval from 20 to 500 mV/s, the peak potential difference remains constant at 58.5 ± 3 mV, with a mid-potential of -0.129 ± 0.003 V, and the peak current ratio of 1.025 ± 0.033. Both cathodic and anodic peak currents depend linearly on the square-root of the scan rate with a linear regression coefficient of $R^2 = 0.999$ and 0.998, respectively. Invoking the Randles–Sevcik Eq. [30], the slope of these lines enabled to estimate the real electrode surface area to be 7.1×10^{-6} m^2, assuming a common diffusion coefficient of 9×10^{-10} m^2 s^{-1}[31–33].

An attempt to shift the electrode reaction to the quasireversible kinetic region was achieved by applying square-wave voltammetry (SWV)[17]. Initially, the electrode reaction was studied at moderate frequency of 25 Hz and a low amplitude of 25 mV, when the electrode kinetic is expected to be within the electrochemically reversible kinetic region (Fig. 5B). The peak potential of the net component is -0.128 V, which is virtually identical with the mid-potential measured with CV, suggesting the reversible character of the electrode reaction. The other voltammetric features of the response shown in Fig. 5B, such as peak potential difference of the cathodic and anodic components, as well as the half-peak width of the net peak align well with the theoretical expectation for a very fast, apparently reversible electrode reaction[17]. Increasing the frequency up to 400 Hz does not affect

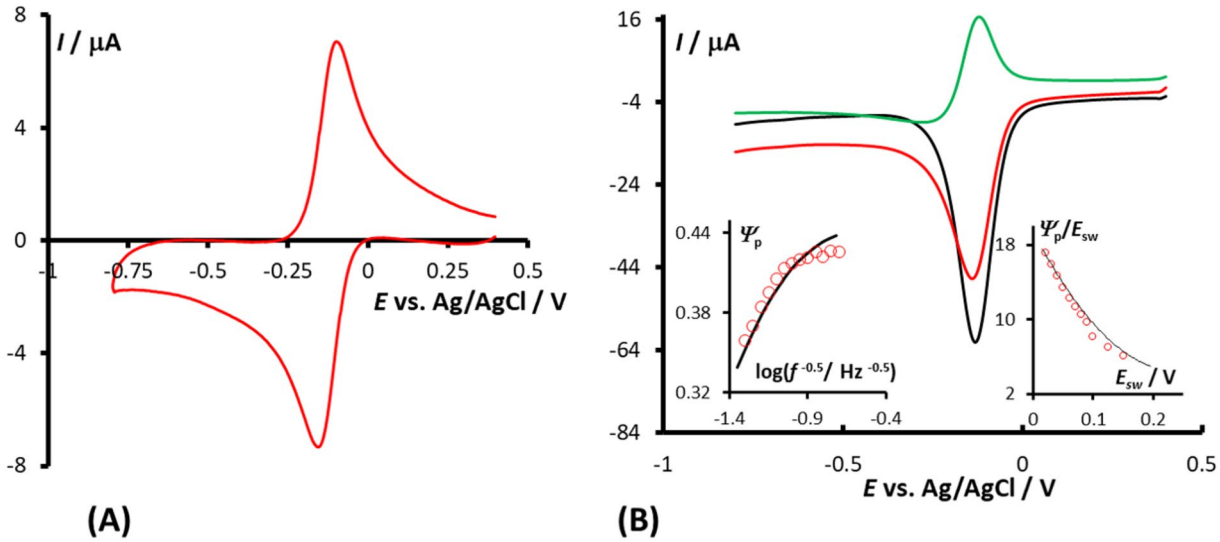

Figure 5. Typical cyclic (**A**) and square-wave voltammogram (**B**) of 1 mmol/L $[Ru(NH_3)_6]Cl_3$ at GCE in 1 mol/L KNO_3 supporting electrolyte at scan rate 20 mV/s and potential increment of 2.44 mV for (**A**) and frequency of 25 Hz, SW amplitude of 25 mV and step potential 5 mV, showing forward (cathodic; red), backward (anodic; blue) and net SW component (black). All curves have been smoothed and in the case of CV background corrected. The left inset of (**B**) shows the dependence of the dimensionless net peak current in SWV on the of the inverse square-root of the frequency. Red circles correspond to the normalized experimental data, while the black line represents the theoretical data simulated for the standard rate constant of 0.05 cm s^{-1} and electron transfer coefficient $\beta = 0.5$. The other conditions for normalisation of the experimental currents are: diffusion coefficient $D = 9 \times 10^{-6}$ cm^2 s^{-1}, stoichiometric number of electrons $n = 1$, and temperature 293.15 K. The right inset of (B) shows the dependency of the amplitude-normalized net peak currents on the SW amplitude. Red circles show experimental data while the black line corresponds to the simulations performed for identical kinetic parameters as in the left inset. The experiments and simulations are conducted at the frequency of 100 Hz.

the net peak potential, which remains at the value of -0.128 V; yet, the peak current does not increase strictly linearly with the square-root of the frequency, implying that the effect of the quasireversible kinetic behaviour commences to be effective, in particular, at frequencies larger than 100 Hz. Let us note that the frequency of 100 Hz corresponds to a typical time window of the voltammetric experiment of 5 ms in SWV.[17] Assuming the same time interval in CV over potential window of, e.g., 0.4 V, would corresponds to the scan rate of 160 V/s.

Thus, at the SW frequencies $f > 100$ Hz, the electrode reaction is gradually shifted from the reversible to the quasireversible kinetic region. The theory of SWV suggest that the dimensionless net peak current is becoming sensitive to the frequency, whereas the net peak potential remains unaffected up to the irreversible kinetic region, which is in excellent accord with the experimental data. The left inset of Fig. 5B shows the dependency of the normalized (dimensionless net peak current) on the parameter $\log\left(\frac{1}{\sqrt{f}}\right)$. Note that the latter parameter $\frac{1}{\sqrt{f}}$ corresponds to the dimensionless electrode kinetic parameter in SWV $\left(\kappa = \frac{k_s}{\sqrt{Df}}\right)$. The red circles in the left inset of Fig. 5B represent the experimental data, which aligns with the theoretically predicted dependence of ψ_p vs. $\log(\frac{1}{\sqrt{f}})$ (black line)[17]. The linearly increasing part of the function ψ_p vs. $\log(\frac{1}{\sqrt{f}})$ is typical for the quasireversible kinetic region. An attempt to fit the experiment with the simulations, results in the best fit with a standard rate constant of $k_s = (0.05 \pm 0.01)$ cm s^{-1}. In addition, kinetic measurements in SWV can be done by means of the amplitude variation at the constant frequency as elaborated in[34]. Applying the method of the amplitude-based quasireversible maximum[35], the fitting of the experimental with the theoretical data is presented in the right inset of Fig. 5B, achieved again with the standard rate constant being within the interval of 0.05 ± 0.02 cm s^{-1}.

This general kinetic characterisation of the ruthenium redox system confirms the well-known fact that it is one of the fastest electrode reactions of a dissolved redox couple studied[36]. Under moderate experimental conditions, as those in Fig. 5A, the electrode reaction is virtually reversible process. The electrode kinetics could be estimated in CV by applying conventional analysis by varying the scan rate over 160 V/s; the artefacts arising from such extreme scan rates are quite predictable, which in reality practically preclude kinetic measurements at a macroscopic electrode. Yet the methodology proposed in this study promises kinetic estimation at mild experimental conditions, i.e., macroscopic electrode and low scan rate, i.e., in conditions when the artefacts arising from uncompensated resistance and charging current can be reasonably neglected. Specifically, for the present experimental conditions and the scan rate of 0.02 V/s, the charging current is estimated to be within the interval from 0.02 to 0.08 µA, whereas the uncompensated resistance in 1 mol/L KNO_3 used as a supporting electrolyte and the distance between the working and reference electrode of 1 cm is estimated to be in the range of 9 mΩ, which is insignificant for distortion of the applied potential sweep.

Let us first study the evolution of the classical convolution current as a function of the potential, corresponding to the initial, cathodic potential scan of the cyclic voltammetric experiment of ruthenium system, which is shown in Fig. 6A. The sigmoid curve is constructed from experimental currents after normalisation, smoothing and background correction for the experiment conducted at low scan rate of 20 mV/s. The convolution current is virtually free of noise, with a half-wave potential of – 0.129 V, which is in excellent agreement with the formal potential estimated from the conventional CV and SWV. Having in hand the convolution currents and applying Eqs. (12) and (13), the genuine anodic and cathodic implicit current components corresponding to the forward scan of the cyclic voltammetry, have been calculated and depicted in Fig. 6B. The shape of the curves is in excellent agreement with the theoretical predictions for a very fast electrode reaction (compare Fig. 6B with 1D). The intensity of both cathodic and anodic current components is an order of magnitude higher than the conventional voltammogram, shown with a blue line in Fig. 6B. The peak potential of both cathodic and anodic implicit current components is identical, located at the formal potential of the electrode reaction, while the peak current ratio is virtually one. Such evolution of current components is typical for very fast, apparently reversible electrode processes, with an electron transfer coefficient equal to 0.5, as illustrated in Fig. 1D. Following the proposed methodology, a differential current component is constructed as a $\Psi_{dif} = \Psi_c - \Psi_a$, which is depicted as an inset of Fig. 6B. The peak current of the differential component is 7.42. Thus, the dimensionless electrode kinetic parameter for the ruthenium system is $\kappa = 7.42$ leading to the standard rate constant $k_s = \kappa\sqrt{\frac{DvF}{RT}} = 0.02$ cm s^{-1}. To the best of our knowledge, this is the only method enabling to estimate such a high standard rate constant at a macroscopic electrode and a single scan rate of 20 mV/s.

To simplify, the previous estimation assumed identical diffusion coefficients for both redox species in the ruthenium system. In a more rigorous approach, different diffusion coefficients should be employed, as discussed in our previous study.[12] In such cases, the implicit anodic and cathodic current components additionally depend on the ratio $\rho = D_R/D_O$, where D_R and D_O are the diffusion coefficients of the reduced and oxidised form, respectively. The work of Compton et al.[31] reports values of 5.3×10^{-6} cm^2/s and 7.3×10^{-6} cm^2/s for Ru(III) and Ru(II), respectively in 0.5 mol/L KNO_3 as a supporting electrolyte. Assuming these values applied under the current experimental conditions, the diffusion coefficient ratio is $\rho = 1.38$, which insignificantly affects the magnitude of the convolution currents Ψ_{con} calculated for each potential in the cyclic voltammograms of the ruthenium system.

More critically, when diffusion coefficients are unequal, the mid-potential E_m estimated from the cyclic voltammograms is $E_m = E^{0'} + \frac{RT}{F} ln\sqrt{\rho}$, differing from the formal potential. Conversely, precise knowledge of the formal potential is crucial for estimating implicit current components (cf. Eqs. (12) and (13) and the definition of parameters a and b therein) through the values of the dimensionless potential ϕ. Adjusting for this, the formal potential of the ruthenium system is estimated at -0.133 V, which is 4 mV more negative than the previously used value of -0.129 V. Revising the standard rate constant by incorporating the ρ parameter[12] and using the corrected formal potential yields again values in the range of 0.02 ± 0.005 cm s^{-1}.

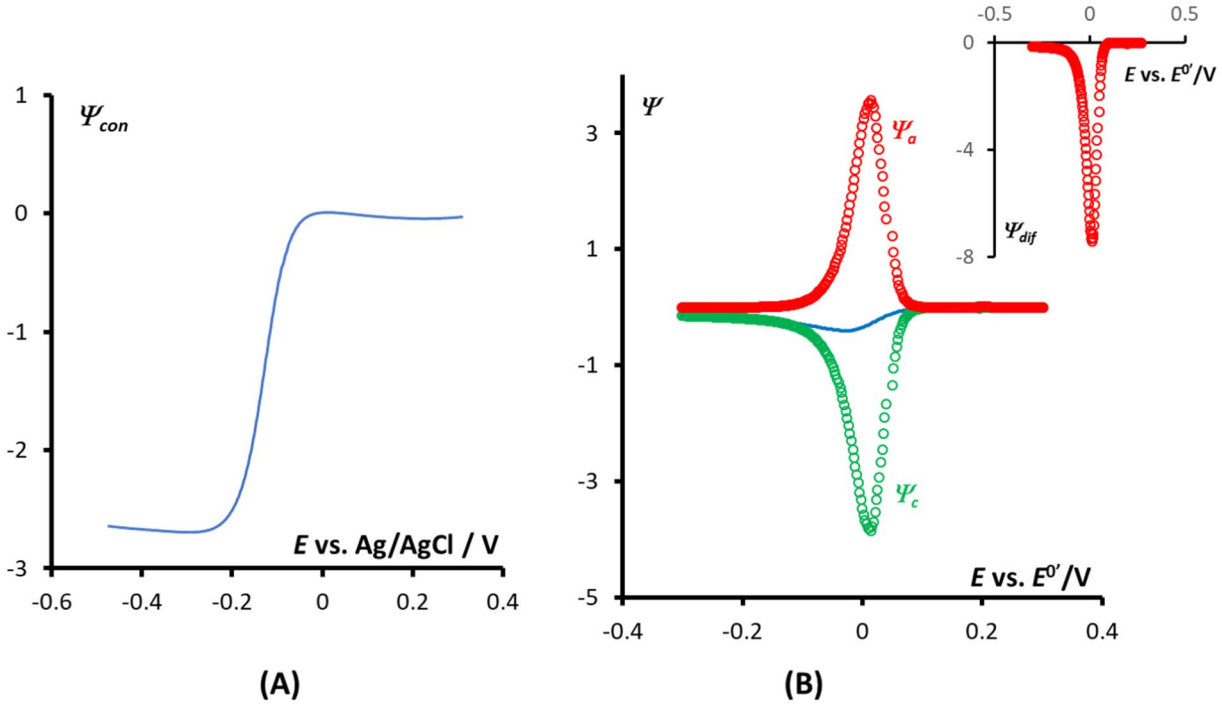

Figure 6. (**A**) Convolution dimensionless current as a function of the electrode potential and (**B**) dimensionless cathodic (green circles) and anodic (red circles) implicit current components as function of the relative potential E vs. $E^{0'}$ of the ruthenium system, corresponding to the forward half-cycle of the cyclic voltammogram shown in Fig. 6B (solid blue line). The inset of panel (**B**) shows the differential current component calculated as a difference between the cathodic and anodic implicit current components. All experimental conditions are identical as in Fig. 5A.

Electrode	Supporting electrolyte	Technique	k_s[cm s^{-1}]	References
Au nanotips	0.5 M KCl	SECM	13.5	[37]
Graphite SPE	0.1 M KCl	CV	0.0025	[38]
GC	1 M KCl	CV	0.127	[39]
Au	0.1 M PBS	EIS	0.390	[40]
Pt (ultramicro electrode)	0.1 M KCl	EIS	0.52	[29]
GC	1 M KNO_3	CV	0.02	This work

Table 1. A selection of standard rate constants estimated for ruthenium redox system.

In Table 1 we are giving a brief summary of literature values for standard rate constants of the ruthenium system. As often happens, the kinetic data differ significantly depending on the method used. Here, our data are supported by an independent estimation using SWV.

Conclusions

Through the straightforward convolution procedure of the actual net current, and with sole prior knowledge of the formal potential of the electrode reaction, implicit anodic and cathodic current components at a given potential can be unequivocally estimated. The numerical calculation of the convolution integral $I_{con} = \int_0^t \frac{I(\tau)}{FA\sqrt{D}} \frac{d\tau}{\sqrt{\pi(t-\tau)}}$ is required, similar to classical convolution voltammetry[13–16]; however, in our proposed method, the focus shifts from analyzing the convolution current as a function of potential and electrode kinetic parameters ($I_{con} = f(E, k_s, \beta)$) as in classical convolution voltammetry[13,14]. Instead, it is employed to unveil implicit anodic and cathodic current components, which represent the common (non-convolutive) current. This approach transforms a simple cyclic voltammogram, measured using the most basic linear sweep potential variation, in a unique way, enabling to uncover, genuine anodic and cathodic, yet implicit, current components.

Delving into the intrinsic meaning of our proposed methodology, one realizes that after measuring the common voltammogram, whose net current is intricately determined by the interplay between mass transfer and electrode kinetics, the convolution procedure of the net current effectively isolates the contributions of mass transfer and electrode kinetics in the overall net current. This allows for the estimation of the rate of very fast, seemingly reversible electrode processes under mild experimental conditions, when very slow scan rates are applied to common, macroscopic electrodes. To our knowledge, this represents a unique achievement, offering a completely new perspective on analyzing electrode processes under voltammetric conditions.

Data availability

Data available on request from the corresponding author VM.

Received: 20 March 2024; Accepted: 16 July 2024
Published online: 27 July 2024

References

1. Marken, F., Neudeck, A. & Bond, A. M. in *Electroanalytical Methods: Guide to Experiments and Applications* (eds Fritz Scholz *et al.*) pp. 57–106 (Springer, Berlin Heidelberg, 2010).
2. Erdey-Grúz, T. & Volmer, M. Zur Theorie der Wasserstoff Überspannung. *Z. Phys. Chem.* **150A**, 203–213. https://doi.org/10.1515/zpch-1930-15020 (1930).
3. Butler, J. A. V. Studies in heterogeneous equilibria: Part II—The kinetic interpretation of the nernst theory of electromotive force. *Trans. Faraday Soc.* **19**, 729–733. https://doi.org/10.1039/TF9241900729 (1924).
4. Inzelt, G. Milestones of the development of kinetics of electrode reactions. *J. Solid State Electrochem.* **15**, 1373–1389. https://doi.org/10.1007/s10008-011-1301-3 (2011).
5. Seeber, R., Zanardi, C. & Inzelt, G. The inherent coupling of charge transfer and mass transport processes: The curious electrochemical reversibility. *ChemTexts* **2**, 8. https://doi.org/10.1007/s40828-016-0027-3 (2016).
6. Dickinson, E. J. F. & Wain, A. J. The Butler-Volmer equation in electrochemical theory: Origins, value, and practical application. *J. Electroanal. Chem.* **872**, 114145. https://doi.org/10.1016/j.jelechem.2020.114145 (2020).
7. Hale, J. M. The potential-dependence and the upper limits of electrochemical rate constants. *J. Electroanal. Chem. Interfacial Electrochem.* **19**, 315–318. https://doi.org/10.1016/S0022-0728(68)80131-7 (1968).
8. Chidsey, C. E. D. Free energy and temperature dependence of electron transfer at the metal-electrolyte interface. *Science* **251**, 919–922. https://doi.org/10.1126/science.251.4996.919 (1991).
9. Feldberg, S. W. Implications of Marcus–Hush theory for steady-state heterogeneous electron transfer at an inlaid disk electrode. *Anal. Chem.* **82**, 5176–5183. https://doi.org/10.1021/ac1004162 (2010).
10. Marcus, R. A. On the theory of oxidation-reduction reactions involving electron transfer I. *J. Chem. Phys.* **24**, 966–978. https://doi.org/10.1063/1.1742723 (1956).
11. Oldham, K. B. & Myland, J. C. On the evaluation and analysis of the Marcus–Hush–Chidsey integral. *J. Electroanal. Chem.* **655**, 65–72. https://doi.org/10.1016/j.jelechem.2011.01.044 (2011).
12. Mirceski, V., Lovric, M., Compton, R. G. & Ullah, N. Revisiting the butler-volmer electrode kinetics: Separating the anodic and cathodic current components of a quasi-reversible electrode reaction in staircase voltammetry. *J. Electroanal. Chem.* **957**, 118111. https://doi.org/10.1016/j.jelechem.2024.118111 (2024).
13. Oldham, K. B. Convolution of voltammograms as a method of chemical analysis. *J. Chem. Soc. Faraday Trans. 1 Phys. Chem. Condens. Phases* **82**, 1099–1104. https://doi.org/10.1039/F19868201099 (1986).
14. Oldham, K. B. Convolution: A general electrochemical procedure implemented by a universal algorithm. *Anal. Chem.* **58**, 2296–2300. https://doi.org/10.1021/ac00124a040 (1986).

15. Mahon, P. J. Convolutive reshaping with applications for voltammetry. *J. Solid State Electrochem.* **13**, 573–582. https://doi.org/10.1007/s10008-008-0664-6 (2009).
16. Bieniasz, L. K. *Modelling Electroanalytical Experiments by the Integral Equation Method* (Springer, Berlin, 2015).
17. Mirceski, V., Komorsky-Lovric, S. & Lovric, M. *Square-Wave Voltammetry: Theory and Application* (Springer, Berlin, 2007).
18. Lovrić, M. & Komorsky-Lovric, Š. Square-wave voltammetry of an adsorbed reactant. *J. Electroanal. Chem. Interfac. Electrochem.* **248**, 239–253. https://doi.org/10.1016/0022-0728(88)85089-7 (1988).
19. Stojek, Z. in *Electroanalytical Methods: Guide to Experiments and Applications* (ed Fritz Scholz) pp 99–110 (Springer, Berlin Heidelberg, 2002).
20. Molina, A. & González, J. *Pulse Voltammetry in Physical Electrochemistry and Electroanalysis Theory and Applications*. 1st ed., (Springer, Heidelberg, 2016).
21. Jakubowska, M., Piech, R., Dzierwa, T., Wcislo, J. & Kubiak, W. W. The evaluation method of smoothing algorithms in voltammetry. *Electroanalysis* **15**, 1729–1736. https://doi.org/10.1002/elan.200302751 (2003).
22. Jakubowska, M. & Kubiak, W. W. Optimization of smoothing process—the method to improve calibration in voltammetry: Part I: simulated voltammograms. *Talanta* **62**, 583–594. https://doi.org/10.1016/j.talanta.2003.09.002 (2004).
23. Yanina, I. Y., Popov, A. P., Bykov, A. V., Meglinski, I. V. & Tuchin, V. V. Monitoring of temperature-mediated phase transitions of adipose tissue by combined optical coherence tomography and Abbe refractometry. *J. Biomed. Opt.* **23**, 016003. https://doi.org/10.1117/1.JBO.23.1.016003 (2018).
24. Bard, A. J., Faulkner, L. R. & White, H. S. *Electrochemical Methods: Fundamentals and Applications* (Wiley, 2022).
25. Randviir, E. P. & Banks, C. E. Electrochemical impedance spectroscopy: An overview of bioanalytical applications. *Anal. Methods* **5**, 1098–1115. https://doi.org/10.1039/C3AY26476A (2013).
26. Nicholson, R. S. Theory and application of cyclic voltammetry for measurement of electrode reaction kinetics. *Anal. Chem.* **37**, 1351–1355. https://doi.org/10.1021/ac60230a016 (1965).
27. Klingler, R. J. & Kochi, J. K. Electron-transfer kinetics from cyclic voltammetry: Quantitative description of electrochemical reversibility. *J. Phys. Chem.* **85**, 1731–1741. https://doi.org/10.1021/j150612a028 (1981).
28. Eisner, U. & Gileadi, E. Anodic oxidation of hydrazine and its derivatives: Part I: The oxidation of hydrazine on gold electrodes in acid solutions. *J. Electroanal. Chem. Interfac. Electrochem.* **28**, 81–92. https://doi.org/10.1016/S0022-0728(70)80284-4 (1970).
29. Vijaikanth, V., Li, G. & Swaddle, T. W. Kinetics of reduction of aqueous hexaammineruthenium(III) Ion at Pt and Au microelectrodes: Electrolyte, temperature, and pressure effects. *Inorg. Chem.* **52**, 2757–2768. https://doi.org/10.1021/ic400062b (2013).
30. Nagaraj, P. S., Deepti, S. N., Shweta, J. M. & Raviraj, M. K. Electrochemical sensor based upon ruthenium doped TiO2 nanoparticles for the determination of flufenamic acid. *J. Electrochem. Soc.* **164**, B3036. https://doi.org/10.1149/2.0031705jes (2016).
31. Wang, Y., Limon-Petersen, J. G. & Compton, R. G. Measurement of the diffusion coefficients of [Ru(NH3)6]3+ and [Ru(NH3)6]2+ in aqueous solution using microelectrode double potential step chronoamperometry. *J. Electroanal. Chem.* **652**, 13–17. https://doi.org/10.1016/j.jelechem.2010.12.011 (2011).
32. Banks, C. E., Compton, R. G., Fisher, A. C. & Henley, I. E. The transport limited currents at insonated electrodes. *Phys. Chem. Chem. Phys.* **6**, 3147–3152. https://doi.org/10.1039/B403751K (2004).
33. Jonathan, M., Madeline, M. & David, W. P. Rapid and direct determination of diffusion coefficients using microelectrode arrays. *J. Electrochem. Soc.* **163**, H672. https://doi.org/10.1149/2.0561608jes (2016).
34. Mirceski, V., Guziejewski, D. & Lisichkov, K. Electrode kinetic measurements with square-wave voltammetry at a constant scan rate. *Electrochim. Acta* **114**, 667–673. https://doi.org/10.1016/j.electacta.2013.10.046 (2013).
35. Mirceski, V., Laborda, E., Guziejewski, D. & Compton, R. G. New approach to electrode kinetic measurements in square-wave voltammetry: Amplitude-based quasireversible maximum. *Anal. Chem.* **85**, 5586–5594. https://doi.org/10.1021/ac4008573 (2013).
36. Levey, K. J., Edwards, M. A., White, H. S. & Macpherson, J. V. Simulation of the cyclic voltammetric response of an outer-sphere redox species with inclusion of electrical double layer structure and ohmic potential drop. *Phys. Chem. Chem. Phys.* **25**, 7832–7846. https://doi.org/10.1039/D3CP00098B (2023).
37. Velmurugan, J., Sun, P. & Mirkin, M. V. Scanning electrochemical microscopy with gold nanotips: The effect of electrode material on electron transfer rates. *J. Phys. Chem. C* **113**, 459–464. https://doi.org/10.1021/jp808632w (2009).
38. Trachioti, M. G., Lazanas, A. C. & Prodromidis, M. I. Shedding light on the calculation of electrode electroactive area and heterogeneous electron transfer rate constants at graphite screen-printed electrodes. *Microchim. Acta* **190**, 251. https://doi.org/10.1007/s00604-023-05832-w (2023).
39. Jarošová, R., De-Sousa-Bezerra, P. M., Munson, C. & Swain, G. M. Assessment of heterogeneous electron-transfer rate constants for soluble redox analytes at tetrahedral amorphous carbon, boron-doped diamond, and glassy carbon electrodes. *Phys. Status Solidi* **213**, 2087–2098. https://doi.org/10.1002/pssa.201600339 (2016).
40. Wieckowska, A., Jablonowska, E., Jaskolowski, M. & Bilewicz, R. Efficient electron transfer through insulating lipid bilayers containing Au clusters. *J. Electroanal. Chem.* **932**, 117261. https://doi.org/10.1016/j.jelechem.2023.117261 (2023).

Acknowledgements

This research was funded in whole or in part by National Science Center, Poland 2020/39/I/ST4/01854. For the purpose of Open Access, the author has applied a CC-BY public copyright licence to any Author Accepted Manuscript (AAM) version arising from this submission.

Author contributions

V.M.: Conceptualization, methodology, data curation, project administration, resources, supervision, writing: original draft, writing: review and editing, funding acquisition; D.G.: Investigation, data curation, validation, writing: review and editing; R.G.: Writing: review and editing.

Competing interests

The authors declare no competing interests.

Additional information

Correspondence and requests for materials should be addressed to V.M.

Reprints and permissions information is available at www.nature.com/reprints.

Publisher's note Springer Nature remains neutral with regard to jurisdictional claims in published maps and institutional affiliations.